LA-7843-PR

Progress Report

C.3

Applied Nuclear Data Research and Development

January 1—March 31, 1979

LOS ALAMOS SCIENTIFIC LABORATORY
Post Office Box 1663 Los Alamos, New Mexico 87545

The four most recent reports in this series, unclassified, are LA-7301-PR, LA-7482-PR, LA-7596-PR, and LA-7722-PR.

This report was not edited by the Technical Information staff.

This work was performed under the auspices of the US Department of Energy's Office of Military Application, Division of Reactor Research and Technology, Office of Basic Energy Sciences, and Office of Fusion Energy; and the Electric Power Research Institute.

UNITED STATES
DEPARTMENT OF ENERGY
CONTRACT W-7405-ENG. 36

LA-7843-PR
Progress Report
Special Distribution
Issued: May 1979

Applied Nuclear Data Research and Development

January 1—March 31, 1979

Compiled by

C. I. Baxman
P. G. Young

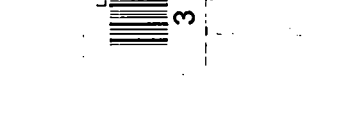

CONTENTS

APPLIED NUCLEAR DATA RESEARCH AND DEVELOPMENT
QUARTERLY PROGRESS REPORT
January 1 - March 31, 1979

Compiled by

C. I. Baxman and P. G. Young

ABSTRACT

This progress report describes the activities of the Los Alamos Nuclear Data Group for the period January 1 through March 31, 1979. The topical content is summarized in the contents.

I. THEORY AND EVALUATION OF NUCLEAR CROSS SECTIONS

A. Neutron-Proton and Proton-Proton Elastic Scattering (D. Dodder)

An R-matrix analysis of proton-proton elastic scattering in the 1-30 MeV energy region has been extended to include neutron-proton scattering over the same range. This analysis assumes charge independence of the R-matrix parameters except for a Coulomb energy shift. This procedure, which has proven satisfactory for a number of few-nucleon systems, suffices here also to fit the data base, which is nearly complete. Preliminary indications are that the neutron-proton angular distribution predictions will differ noticeably but not substantially from those in ENDF/B-V.

B. Pion-Nucleon Elastic Scattering (D. Dodder)

New, preliminary $p(\pi^+,\pi^+)p$ and $p(\pi^-,\pi^-)p$ data from 30 to 90 MeV from the particle physics group at LAMPF have been incorporated in the R-matrix analysis. The new $p(\pi^+,\pi^+)p$ data are in substantial agreement with the previous analysis and serve chiefly to improve its precision. The new $p(\pi^-,\pi^-)p$ data are much more precise than the previous data and serve to determine phase parameters that were very poorly determined before. They also verify previous data selection made on the basis of the R-matrix analysis. When the final version of the new data is

incorporated in the analysis, it will allow new, more accurate scattering length determinations to compare with theoretical prediction. It will also give a new set of predictions of the cross sections for those processes. These predictions are used for calibrating a large number of nuclear structure measurements at LAMPF.

C. Scattering Lengths for n-^{3}He and n-T (G. M. Hale and D. Dodder)

One aspect of the four-nucleon problem that was pointed out in a paper by Rauch[1] at the International Conference on Few-Body Systems and Nuclear Forces held recently in Graz, Austria, is the rather uncertain experimental situation concerning n-^{3}He and n-T (s-wave) scattering lengths. Despite the fact that Rauch's group[1] has determined the coherent scattering length for n-^{3}He quite well ($a_c = 4.28 \pm 0.05$ fm), its decomposition into singlet (a_s) and triplet (a_t) scattering lengths remains rather uncertain. Moreover, for the case of n-T, no combination of a_s and a_t accounts simultaneously for Donaldson's[2] value of the coherent scattering length ($a_c = 3.75 \pm 0.23$ fm) and various measurements of the low-energy scattering cross section within experimental errors.

We have extracted predictions for n-^{3}He and n-T scattering lengths from our charge-independent R-matrix analysis of the nucleon-trinucleon reactions. This analysis, a minor variation of the one reported at Graz,[3] uses essentially the same isospin-1 parameters to describe p-^{3}He and n-T scattering as well as the isospin-1 part of the reactions possible among p-T and n-^{3}He. Charge-independent constraints simply relate the widths in the p-T and n-^{3}He channels for both T = 1 and T = 0 levels.

Calculated values of the scattering lengths are given in Table I. These are predictions in the sense that they result from analyzing measurements from all the nucleon-trinucleon reactions over a wide range of energy in a charge-independent framework but without direct experimental information about the scattering lengths. Therefore, it is quite satisfying to obtain exact agreement with Rauch's measurement of the coherent scattering length for n-^{3}He. For the case of n-T, our values of a_s and a_t give a coherent scattering length barely within the lower limit of Donaldson's measurement,[2] and a zero-energy elastic scattering cross section of 1.6 b, which is the upper limit of a measurement by Vertebnyi.[4] While the calculated values given in the table are preliminary and have no associated uncertainties, we do not expect large changes or large uncertainties in the final values. This improved determination of the singlet and triplet

TABLE I

SCATTERING LENGTHS (in fm) FOR n-^{3}He AND n-T

	a_s	a_t	a_c
n-^{3}He, calc.	7.37-i4.42	3.25-i0.006	4.28
n-^{3}He, meas.[1]			4.28 $\pm$ 0.05
n-T, calc.	3.68	3.52	3.56
n-T, meas.[2]			3.75 $\pm$ 0.23

scattering lengths for n-^{3}He and n-T, particularly that for the strongly attractive and highly absorptive singlet state in n-^{3}He, should provide a more sensitive test of microscopic calculations for the four-nucleon system.

D. New Evaluation of Elastic and Inelastic Scattering for ^{9}Be (P. G. Young)

A new evaluation of neutron elastic and inelastic scattering for ^{9}Be has been completed for the neutron energy range up to 20 MeV. The new analysis includes extensive new measurements from the Triangle Universities National Laboratory[5] (TUNL) and Los Alamos Scientific Laboratory[6] (LASL) as well as a large collection of older measurements.[7] The evaluated data are represented as Legendre coefficients, reaching an order of ℓ_{max} = 12 at energies from 15-20 MeV.

Below 1.5 MeV, the evaluated elastic angular distributions are based mainly on the measurements of Lane[8,9] and Langsdorf[10] as indicated in Fig. 1. A composite of measurements[7] was used in the evaluation from 1.5-7 MeV, and the new Duke results[5] were emphasized from 7-15 MeV (see Figs. 2 and 3). At 15 MeV, Legendre coefficients from optical-model calculations using the Wilmore and Hodgson[11] parameters were renormalized (slightly) to match the experimental data and used to extend the evaluation to 20 MeV.

The evaluated Legendre coefficients for inelastic scattering to a cluster of states near E_x = 2.43 MeV in ^{9}Be are shown in Fig. 4. Again, the evaluation is based mainly on the TUNL measurements.[5]

The results of this analysis have been incorporated into the LASL evaluation[12] for ^{9}Be and will be available for distribution through the ENDF/A library at the Brookhaven National Nuclear Data Center and from the Radiation Shielding Information Center at Oak Ridge.

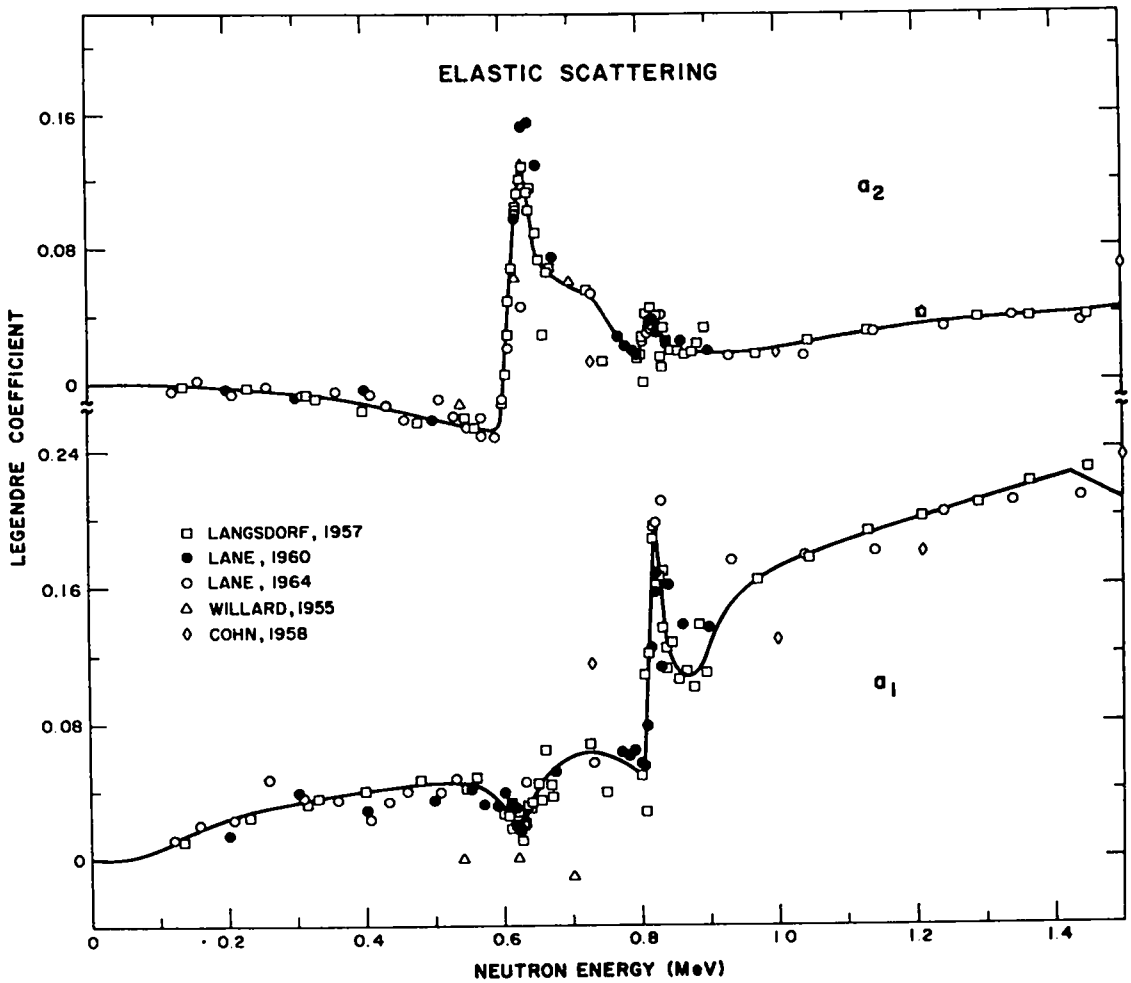

Fig. 1.
Legendre coefficients for n-^{9}Be elastic scattering from 0 to 1.5 MeV. The solid curves represent the evaluation, and the experimental points are from fits to data in Refs. 7-10.

E. Calculation of Neutron-Induced Cross Sections on Isotopes of Iridium (E. D. Arthur)

We have completed preequilibrium statistical-model calculations of neutron-induced reaction cross sections on ^{193}Ir in the energy region between 0.05 and 20 MeV. This effort is an extension of our earlier calculations[13] of ^{191}Ir and ^{193}Ir capture cross sections.

Cross sections were calculated using the GNASH[14] and COMNUC[15] Hauser-Feshbach statistical-model codes. The neutron optical-model parameters of Table II were used and are based on a set derived from fits[16] to total cross sections and resonance data for iridium isotopes. The present set has been modified slightly so

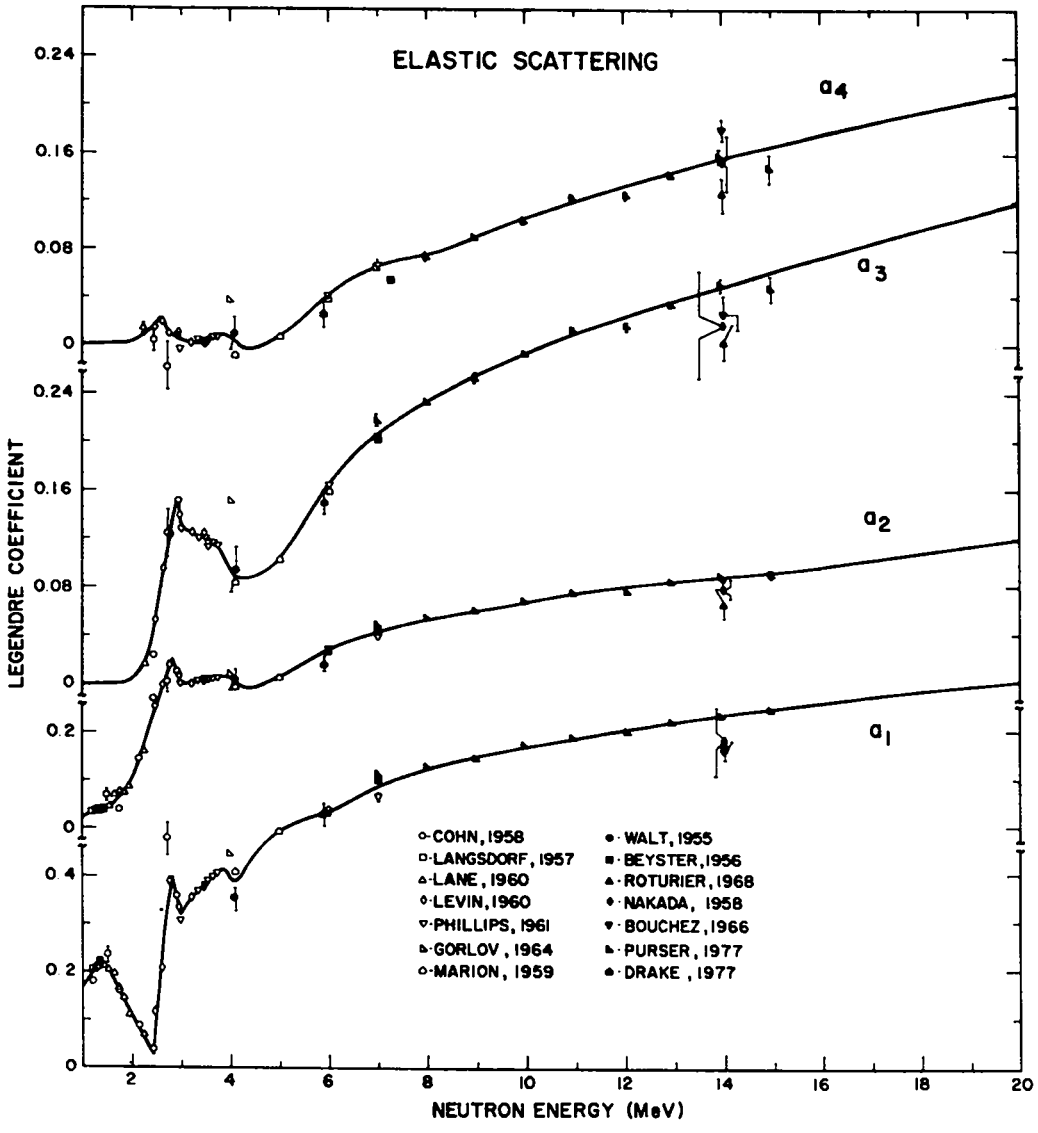

Fig. 2.
Legendre coefficients for ℓ = 1-4 over the energy range 1 to 20 MeV. The solid curves represent the evaluation, and the experimental points are from fits to data in Refs. 5-10.

that the calculated reaction cross section would be increased above 10 MeV. This was necessary in order to reproduce the ^{193}Ir(n,n')^{193m}Ir data of Bayhurst.[17] To describe gamma-ray emission, we used gamma-ray strength functions determined from fits to ^{191}Ir and ^{193}Ir capture cross sections. Reliable data[18] exist for these (n,γ) reactions, and we believe the extracted strength functions can be used with confidence to normalize the amount of gamma-ray competition to neutron emission.

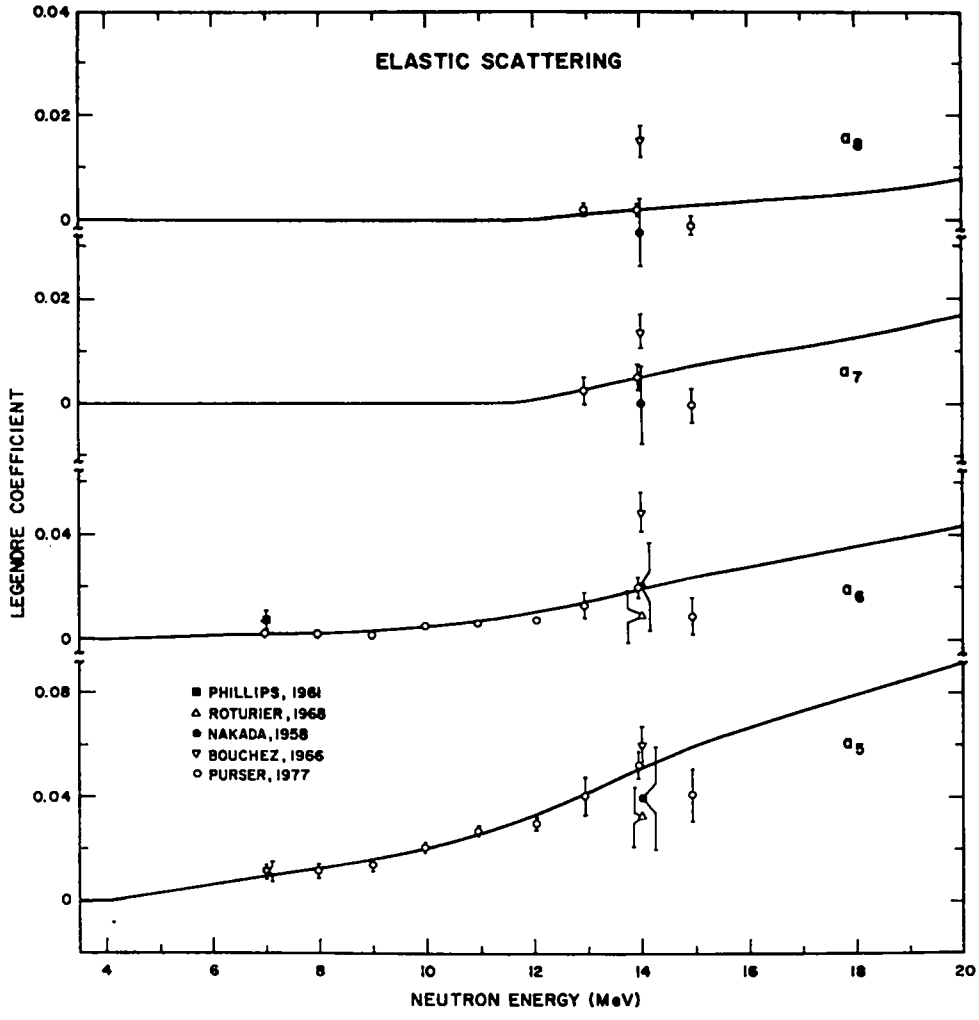

Fig. 3.
Legendre coefficients for ℓ = 5-8 over the energy range 1 to 20 MeV. The solid curves represent the evaluation, and the experimental points are from fits to data in Refs. 5-10.

Figure 5 compares our calculated cross sections to experimental data for neutron reactions on ^{193}Ir. The open diamonds are the ^{193}Ir(n,n')^{193m}Ir data of Bayhurst and should be compared to the solid curve representing the calculated cross section for that reaction. Most of the other experimental points are measurements of the ^{193}Ir(n,2n)$^{192g+ml}$Ir reaction and should be compared to the dashed curve. This comparison indicates that the present gamma-ray and neutron parameters produce calculated results in agreement with available data for ^{193}Ir. Efforts are now underway to use these parameters for the calculation of neutron-

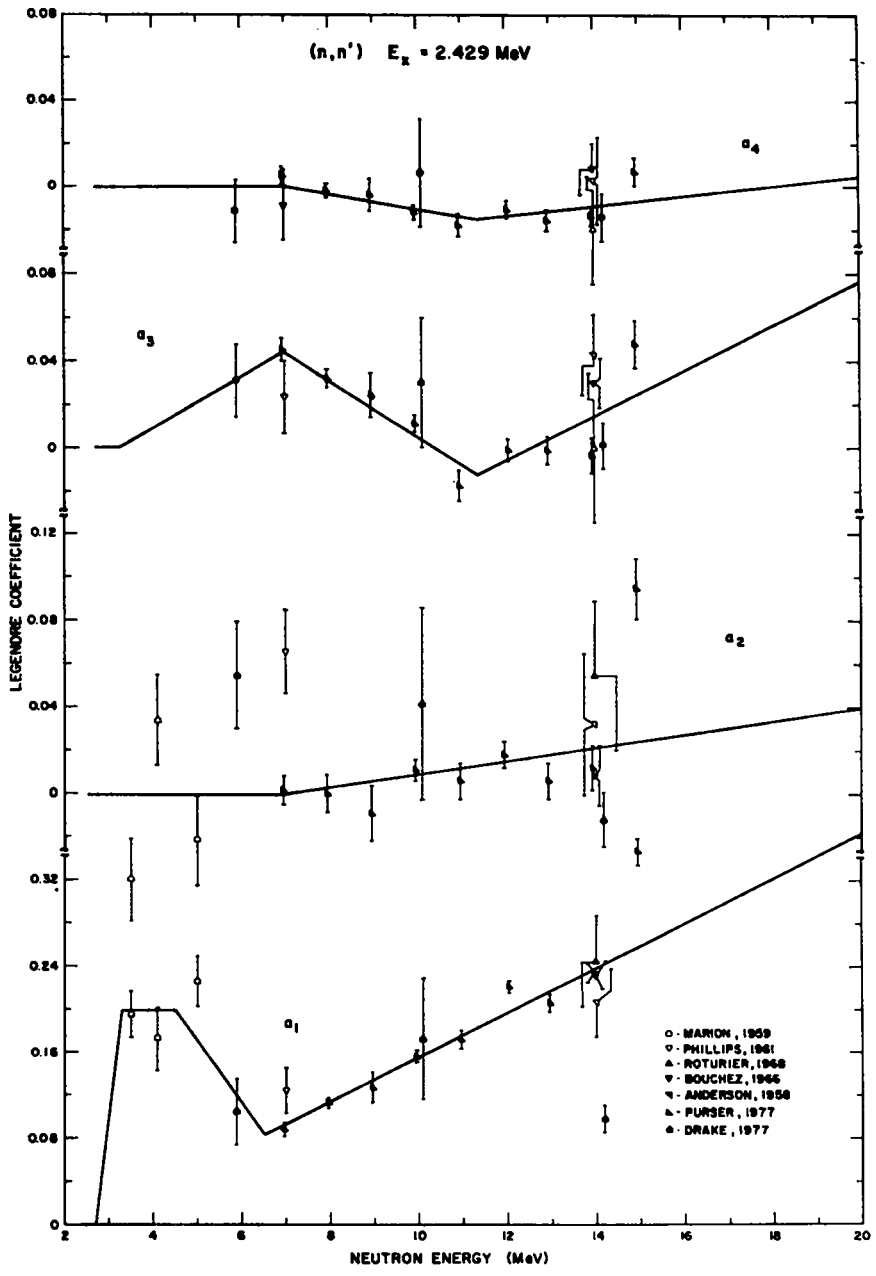

Fig. 4.
Legendre coefficients for n-^{9}Be inelastic scattering to states near E_x = 2.43 MeV. The solid curves represent the evaluation, and the experimental points are from fits to data in Refs. 5-7.

induced reactions on ^{191}Ir. A summary of the reaction cross sections calculated or evaluated for ^{193}Ir appears in Table III.

TABLE II

NEUTRON OPTICAL PARAMETERS USED FOR n + ^{193}Ir CALCULATIONS

Strength (MeV)	r(fm)	a(fm)
V = 44.25 - 0.05E	1.31	0.497
W (Gaussian) = 11.1 + 0.4E	1.313	1.15
V_{so} = 7	1.31	0.497

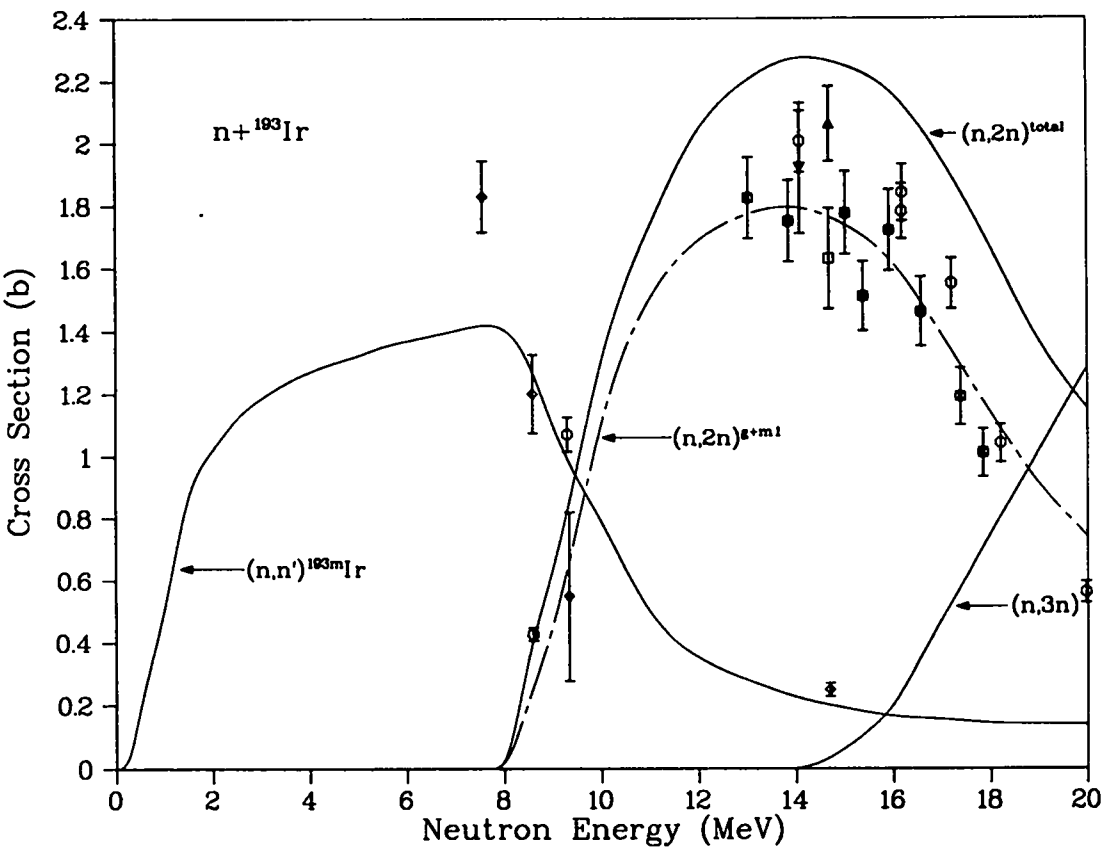

Fig. 5.
Comparison of calculated and experimental data for the $^{193}Ir(n,n')$, (n,2n), and (n,3n) reactions.

TABLE III

Q VALUES AND THRESHOLDS FOR ^{193}Ir REACTIONS

MT	Reaction	Q (MeV)	E_{th} (MeV)
4	^{193}Ir(n,n')^{193}Ir	-0.7301	0.7339
16	^{193}Ir(n,2n)^{192}Ir	-7.772	7.812
16	^{193}Ir(n,2n)$^{192g+m1}$Ir	-7.772	7.812
16	^{193}Ir(n,2n)^{192m2}Ir	-7.873	7.914
17	^{193}Ir(n,3n)^{191}Ir	-13.97	14.64
53	^{193}Ir(n,n')^{193m}Ir	-0.803	0.807
102	^{193}Ir(n,γ)^{194}Ir	6.066	0

F. Calculation of Neutron Cross Sections for ^{184}W (E. D. Arthur)

Earlier we described efforts[19] to determine parameters for use in nuclear-model calculations of neutron-induced reactions on tungsten isotopes. Afterwards a mistake was discovered in the GNASH code that necessitated a redetermination of these parameters. Here we describe new parameter sets to be used for ^{184}W calculations.

Since the tungsten isotopes are deformed, we decided to determine the total direct inelastic cross section using coupled-channel calculations and then to subtract it from the experimental total cross section to produce results that were fit using spherical optical-model parameters. By doing so, the direct component to the total reaction cross section can perhaps be separated, and the remainder can be described using realistic spherical parameters.

For ^{184}W we took a recent evaluation[20] of the total cross section based on measurements of Guenther[21] as well as those of Foster.[22] From this we subtracted direct inelastic scattering cross sections to the 2^+ and 4^+ states calculated with JUPITOR and the Delaroche[23] parameter set. The results were fit by adjusting the spherical parameters determined earlier and are given in Table IV.

Gamma-ray competition can be important, especially around (n,2n) and (n,3n) thresholds. To describe gamma-ray competition, we have used gamma-ray strength functions determined from fits to ^{182,183,184,186}W(n,γ) cross sections.

TABLE IV

SPHERICAL OPTICAL MODEL PARAMETERS n + ^{184}W

Strength (MeV)	r(fm)	a(fm)
$V = 55.2 - 0.13E$	1.1	0.45
$W_D = 5.2 + 0.35E$ (Saxon Derivative)	1.409	0.4
$W_D = 7.3$ for $E_n > 6$ MeV		
$V_{so} = 6.2$	1.01	0.75

Figures 6 and 7 illustrate two differing data types we felt it was necessary to reproduce if the resulting parameters were to be used with confidence in regions lacking in experimental data. Figure 6 shows the total, elastic, and inelastic scattering cross sections calculated with the present spherical parameters through use of the Hauser-Feshbach code COMNUC compared to the results of Guenther et al.[21] For the 0.11 MeV (2^+) and 0.365 (4^+) states, inelastic scattering cross sections from the coupled-channel calculation were added to the Hauser-Feshbach results. Figure 7 compares the GNASH calculated (n,2n) cross sections to the data of Frehaut.[24] It is apparent that the set of neutron and gamma-ray parameters determined here reproduces these two widely different types of experimental data available for the ^{184}W nucleus.

A similar effort is now underway to determine parameter sets for ^{182}W, ^{183}W, and ^{186}W.

G. Calculation of Prompt Fission Neutron Spectra [D. G. Madland and J. R. Nix (T-9)]

The prompt fission neutron spectrum calculations that we have reported thus far[25,26] have been made under the assumption of a constant cross section for the inverse process of compound nucleus formation. We have begun a study of the influence of an energy-dependent compound-nucleus-formation cross section as calculated, for example, using a phenomenological optical-model potential. At this time, the modification of the code FISPEK[26] to accurately calculate the laboratory prompt fission neutron spectrum in this circumstance has been completed. A summary of the code modification follows.

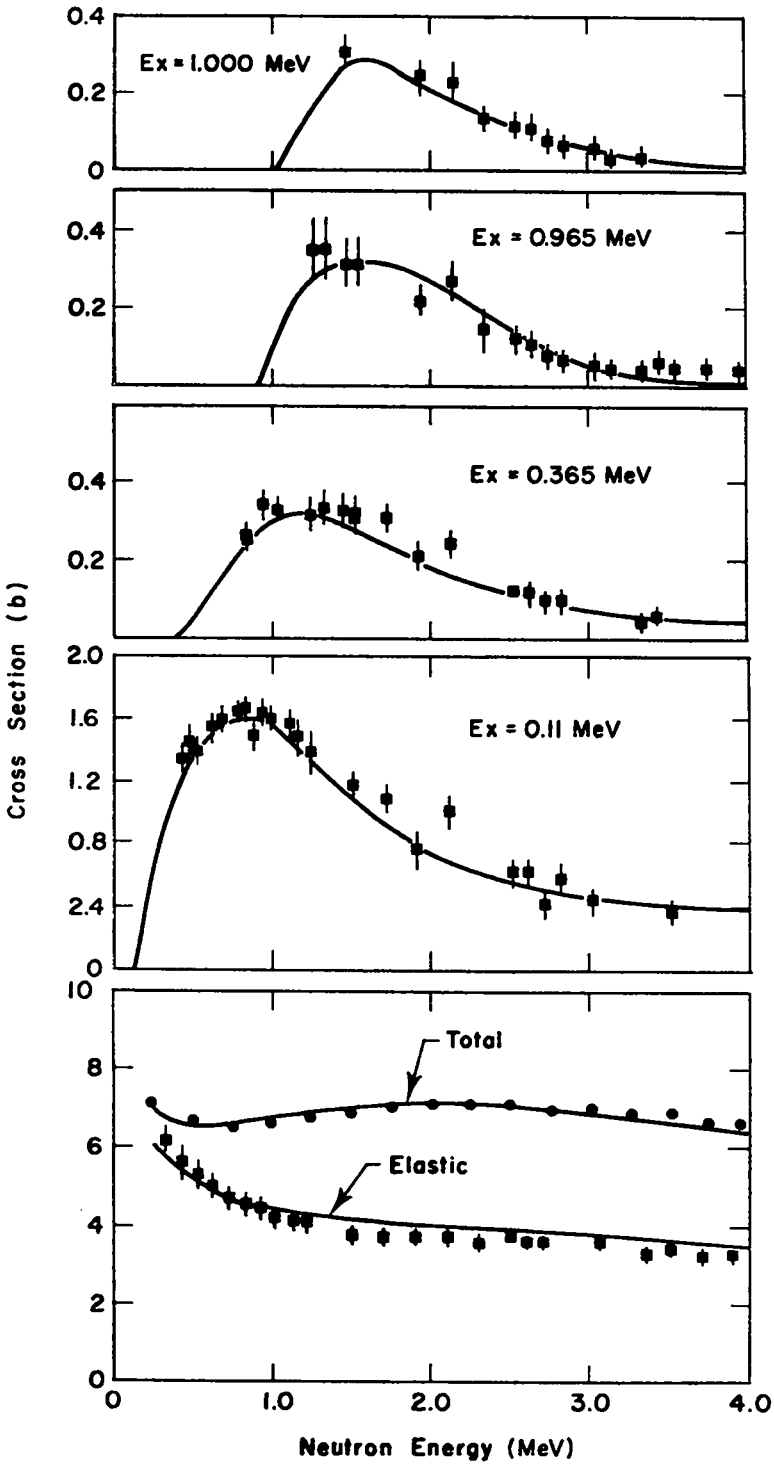

Fig. 6.
Present calculated values for the total, elastic, and certain inelastic scattering cross sections are compared to the Guenther data for ^{184}W.

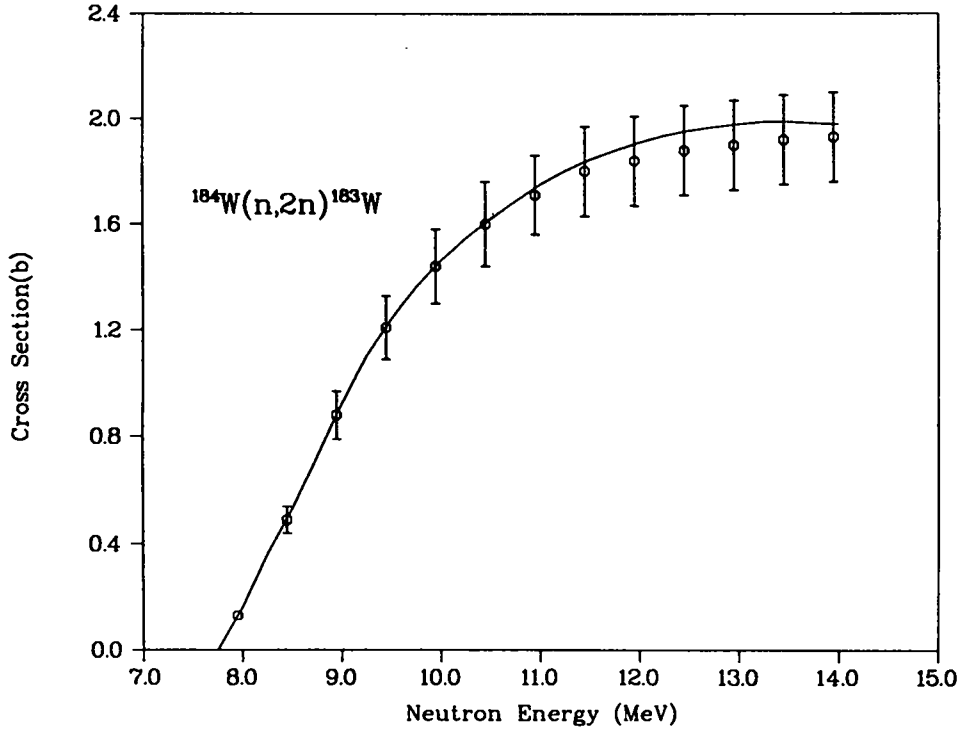

Fig. 7.
The calculated $^{184}W(n,2n)$ cross section is compared to the data of Frehaut.

The laboratory spectrum N(E) is given by

$$N(E) = (1/4\sqrt{E_f}) \int_{S_1}^{S_2} (1/\sqrt{\varepsilon}) \Phi(\varepsilon) d\varepsilon \quad , \tag{1}$$

where E = laboratory neutron energy, ε = center-of-mass neutron energy, E_f = fission fragment average kinetic energy per nucleon, $S_{2,1} = (\sqrt{E} \pm \sqrt{E_f})^2$, and $\Phi(\varepsilon)$ = temperature integrated center-of-mass neutron spectrum.

The temperature integrated center-of-mass spectrum is given by

$$\Phi(\varepsilon) = \int_0^\infty \phi(\varepsilon) P(T) dT \quad , \tag{2}$$

where $\phi(\varepsilon)$ = single temperature center-of-mass evaporation spectrum, T = nuclear temperature, and P(T) = nuclear temperature distribution.

The single temperature center-of-mass spectrum is given by

$$\phi(\varepsilon) = C(T)\varepsilon\sigma(\varepsilon)\exp(-\varepsilon/T) \quad , \tag{3}$$

where $C(T)$ = normalization integral and $\sigma(\varepsilon)$ = energy-dependent compound-nucleus-formation cross section for the inverse process.

The normalization integral is given by

$$C(T) = \left[\int_0^\infty \nu\sigma(\nu)\exp(-\nu/T)d\nu\right]^{-1} \quad , \tag{4}$$

and the temperature distribution is

$$P(T) = \begin{cases} 2T/T_m^2 & T \leqslant T_m \\ 0 & T > T_m \end{cases} \quad , \tag{5}$$

where T_m is the maximum nuclear temperature.[25,26]

If $\sigma(\varepsilon)$ is constant, the integration of Eq. (1) can be done exactly in terms of the exponential integral and the incomplete gamma function, as shown in Refs. 25 and 26. In the present case an optical-model calculation is performed to obtain the energy-dependent reaction cross section for an array of approximately 75 center-of-mass energies spanning the range $\sim$0.5 keV to $\sim$35 MeV. This array is read into FISPEK where a cubic spline fit is obtained using a differentiated four-point Lagrangian interpolation formula to evaluate the first derivative at the array end points. The spline coefficients are stored in another array and are used to calculate $\sigma(\varepsilon)$ for $\sim$1 keV $\leqslant \varepsilon \leqslant \sim$30 MeV. For $\varepsilon \leqslant$ 1 keV, or wherever a $1/\sqrt{\varepsilon}$ behavior is established, the optical model reaction cross sections are fit to the expression $\sigma(\varepsilon) = \sigma_0 + \sigma_1/\sqrt{\varepsilon}$, which is then used for all lower values of ε. A constant value of $\sigma(\varepsilon)$ is used for ε values greater than $\sim$30 MeV.

Gaussian quadrature is used to evaluate the three integrals involved in Eq. (1). Gauss-Laguerre quadrature of order m_1 is used to evaluate the normalization integral $\hat{C}(T)$; Gauss-Legendre quadrature of order m_2 is used to evaluate the temperature integrated spectrum $\hat{\Phi}(\varepsilon)$, and it is also used with order m_3 to evaluate

the final integral for $\hat{N}(E)$. The quadrature order can be independently varied for each integration performed in a given calculation. The subroutines containing the weights and abscissas for the Gaussian integration accommodate quadrature orders of $4 \leqslant m_1, m_2, m_3 \leqslant 32$, in unit steps. Finally, we note that the $\hat{C}(T)$ and $\hat{\Phi}(\varepsilon)$ integrals are performed in the same loop instead of sequentially, to minimize the propagation of numerical inaccuracies.

The first test of the modified FISPEK was to use an array of constant compound-nucleus-formation cross-section values in order to reproduce the exact calculation[25,26] as well as to determine convergence rates and computational times. The results are summarized in Table V. If existing measurement uncertainties (2-10%) are the criteron to determine quadrature order, then order 8-16 would appear to be more than sufficient. Close comparisons with other calculations may require order 16-32.

The second test was to use an array of compound-nucleus-formation cross sections generated using a phenomenological spherical optical potential.[27] The results, summarized in Table VI, imply that order 16 or greater should probably be used in all energy-dependent cross-section calculations.

Comparisons with experimental data using energy-dependent compound-nucleus formation cross sections is now proceeding.

II. NUCLEAR CROSS SECTION PROCESSING

A. Coupled Sets for Neutron and Photon Transport Calculations (R. J. Barrett and R. E. MacFarlane)

A compact and easy to use set of coupled cross sections has been generated from the MATXS1 30 x 12 cross-section library using TRANSX. These multigroup constants are available on T02 photostore as six different files. PROM contains prompt coupled transport tables in FIDO format for the 73 materials contained in Table VII. The materials marked with an "a" include photon production data; the photon-production positions for the others contain zeroes. STDST contains steady-state transfer tables in FIDO format for the materials marked with a "b" in Table VII. These were obtained from the prompt tables by adding in important activation and fission-product photons. SLFSD contains self-shielded cross sections for several isotopes. EDIT contains cross sections useful for editing against neutron and photon fluxes to obtain system-response functions. The set includes prompt heat, steady-state total heat, gas production, parasitic absorption, depletion, (n,2n), (n,3n), capture, fission, $\nu\sigma_f$, and total cross sections. These

TABLE V

NUMERICAL INTEGRATION CONVERGENCE PROPERTIES IN THE CASE OF A CONSTANT COMPOUND-NUCLEUS-FORMATION CROSS SECTION

E (MeV) \ M	4 (10 s)	8 (29 s)	16 (71 s)	32 (218 s)
0.001	1.010941	1.000014	1.000002	1.000000
0.010	1.009601	0.999921	1.000002	1.000000
0.100	0.998648	0.999904	0.999999	1.000000
1.00	0.996907	0.999310	1.000059	0.999998
10.0	0.984052	1.000000	1.000000	1.000000

Ratio of the laboratory spectrum obtained by Gaussian quadrature numerical integration $\hat{N}(E)$ and the exact solution $N(E)$ as a function of the quadrature order M and the laboratory emission energy E for the case of a constant compound-nucleus-formation cross section. M represents the value of the set (m_1,m_2,m_3) discussed in the text. The calculation times are for 186 values of E using a CDC-6600.

TABLE VI

NUMERICAL INTEGRATION CONVERGENCE PROPERTIES IN THE CASE OF AN ENERGY-DEPENDENT COMPOUND-NUCLEUS-FORMATION CROSS SECTION

E (MeV) \ M	4 (10 s)	8 (25 s)	16 (72 s)	31 (215 s)	32 (233 s)
0.001	1.013839	1.006650	1.000152	1.000000	1
0.010	1.012978	1.006541	1.000151	0.999999	1
0.100	1.005110	1.006289	1.000142	1.000000	1
1.00	1.065947	1.002880	1.000158	0.999998	1
10.0	0.966906	1.010113	1.000643	0.999999	1

Ratio of the laboratory spectrum obtained by Gaussian quadrature numerical integration of order M to that obtained for order 32 for several values of the laboratory emission energy E. The compound-nucleus-formation cross section used in the calculations was obtained using a spherical optical model potential as described in the text. M represents the value of the set (m_1,m_2,m_3) discussed in the text. The calculation times are for 186 values of E using a CDC-7600.

TABLE VII

MATERIALS IN COUPLED CROSS-SECTION LIBRARY

H-1[a]	O-16[a]	Ni[a,b]	Th-232[b]	Am-241
H-2[a]	F-19[a]	Cu[a,b]	Pa-233	Am-243
H-3	Na-23[a,b]	ZIRC2	U-233[b]	Cm-244
He-3	Mg[a]	Nb-93[a,b]	U-234	Cm-245[a]
He-4	Al-27[a]	Mo[a,b]	U-235[a,b]	Cm-246[a]
Li-6[a]	Si[a]	Rh-103	U-236	Cm-247[a]
Li-6A[a]	Cl[a]	Ag-107	U-237[a]	Cm-248[a]
Li-7[a]	K[a]	Ag-109	U-238[a,b]	Cf-249[b]
Be-9[a,b]	Ca[a]	Cd	U-239[a]	Cf-250[a]
Be-9A[a,b]	Ti[a]	Ta-181[a]	Np-237	Cf-251[a]
B-10[a]	V[a]	W[a]	Pu-238	Cf-252[a]
B-11[b]	Cr[a,b]	Re-185	Pu-239[a,b]	Stainless[a,b]
C-12[a]	Mn-55[a]	Re-187	Pu-240[a,b]	Concrete[a,b]
C-12A[a]	Fe[a,b]	Au-197	Pu-241[b]	
N-14[a]	Co-59[a]	Pb[a]	Pu-242	

[a]Includes photon-production data.

[b]Steady-state table available.

These numbers are given in a simple 6E12.5 format for ease in editing. PMTCHI contains prompt fission spectra (χ) for the 26 fissionable isotopes. STSCHI contains steady-state χ vectors for seven of the isotopes that have delayed neutron data available in ENDF/B-IV. The χ vectors are in 6E12.5 format. This library is described in more detail elsewhere;[28] it should be useful for many applications where self-shielding is not important.

B. NJOY Development (R. E. MacFarlane and R. M. Boicourt)

A new version of NJOY dated April 1978 has been produced and is available for release. This version incorporates changes suggested by L. Reed of the National Energy Software Center (formerly Argonne Code Center) and includes the discrete-angle treatment of thermal scattering described previously.[29] In addition, this version contains no duplicate subroutine or common block names. Errors were fixed in the free-form input of Hollerith data, the reconstruction of

multilevel Breit-Wigner cross sections in RECONR, and the upper energy limit for multigroup fission spectra. Finally, the accuracy of the angular quadrature for two-body scattering and the energy grid for the weight function were improved in GROUPR.

This version does not include damage energy calculation (Sec. II. C. below) or the new pointwise flux calculator (Sec. II. D. below). Changes in the unresolved calculation are anticipated in the near future.

C. Radiation Damage Cross Sections (R. E. MacFarlane)

Damage to materials caused by neutron irradiation is an important design consideration in fission reactors and is expected to be an even more important problem in fusion power systems. There are many radiation effects that may cause damage; for example, direct heating, gas production such as helium embrittlement, and the production of lattice defects. The first two processes are already handled by the NJOY processing system. During this quarter, a preliminary capability to compute lattice damage has been added.

The dominant source of lattice damage caused by neutrons is the displacement of atoms from their normal positions caused by the primary recoil nucleus as it slows down in the lattice. The energy available to displace atoms depends on the recoil spectrum and the partition of recoil energy between electronic excitations and atomic motion. NJOY uses a formula for this partition given by Robinson[30] based on the electronic screening theory of Lindhard.[31]

The main burden of the calculation is the determination of the primary recoil spectrum from ENDF/B data. For the two-body reactions (elastic and discrete-level inelastic), this can be done very accurately using

$$T(E,\mu) = \frac{AE}{(A+1)^2} \quad (1-2M\mu + M^2) \quad , \tag{6}$$

where E is the incident neutron energy, μ is the center-of-mass scattering cosine, A is the atomic weight ratio, and the effective mass is given by

$$M = \sqrt{1 - \frac{A+1}{A} \frac{(-Q)}{E}} \quad , \tag{7}$$

where -Q is the energy of the discrete level. The damage cross section (in eV x barns) due to this reaction is then obtained from

$$D(E) = \sigma(E) \int_{-1}^{1} f(E,\mu)P(T)d\mu \quad , \tag{8}$$

where f is the angular distribution from ENDF/B File 4, P is the Robinson partition function, and the integration is performed using 20-point Gaussian quadrature. Discrete (n,n') particle reactions are handled in the same way at present; that is, LR flags are ignored.

Continuum (n,n') reactions give a recoil spectrum of

$$T = \frac{1}{A} \left(E-2\sqrt{EE'}\,\mu+E'\right) \quad , \tag{9}$$

where E' is the secondary neutron energy, μ is the lab cosine, and photon momentum has been neglected. This function is converted to a damage cross section using

$$D(E) = \sigma(E) \int_{0}^{\infty} dE' \int_{-1}^{1} d\mu\, f(E,\mu)g(E\rightarrow E')P(T) \quad , \tag{10}$$

where g is the secondary-energy distribution from ENDF/B File 5. All other continuum reactions are handled in the same way at present; this includes (n,2n), (n,n')p, etc. Radiative capture is computed using

$$T = \frac{E}{A+1} \, , \tag{11}$$

and (n,particle) reactions use

$$T = \frac{1}{A+1} \left(E^*-2\sqrt{aE^*E_a}\,\mu+aE_a\right) \quad , \tag{12}$$

where a is the mass ratio of the emitted particle, E* is given by

$$E^* = \frac{(A+1-a)E}{A+1} \quad , \tag{13}$$

and the particle energy is approximated as being equal to the smaller of the available energy

$$Q + \frac{AE}{A+1} \quad , \tag{14}$$

or the Coulomb barrier energy

$$\frac{1.029 \times 10^6 \, zZ}{a^{1/3} + A^{1/3}} \text{ (in eV)} \quad , \tag{15}$$

where z is the charge of the emitted particle. A more accurate method may become possible in the future when ENDF/B incorporates more charged-particle spectrum information. The angular distribution is taken to be isotropic in the lab (this will be a poor approximation for energies large with respect to the Coulomb barrier).

This methodology has been incorporated into the HEATR module of NJOY. Results are in good agreement with earlier codes,[32,33] except that NJOY gets larger damage cross sections for (n,particle) reactions because the other codes use an evaporation spectrum that allows a large fraction of the emitted particles to come out with energies below the Coulomb-barrier energy. The damage energy-production cross sections are written on the point-ENDF (PENDF) file just like the heat-production cross sections already produced by HEATR. They are, therefore, available for group-averaging, plotting, and formatting for convenient use as response functions in neutron transport codes.

D. The NJOY Flux Calculator and Intermediate Resonance Effects (R. E. MacFarlane)

Comparison between NJOY-generated cross sections in the 2-200 eV range with those generated by other codes have shown large differences in self-shielding.[34]

In order to discover the source of these differences, a careful analysis of the codes and methods used in this energy range has been started.

Thermal reactor cell codes like EPRI-CELL and EPRI-CPM rely on equivalence principles stating that the cross sections for the actual heterogeneous arrangement of fuel, clad, and moderator are equivalent to the cross sections in a particular homogeneous system. As an example, consider a pin of ^{238}U immersed in water. The fission neutrons appear at high energies, escape from the pin, slow down in the moderator (giving a 1/E flux), and are absorbed by resonances in the pin. The resonance absorption is equivalent to the absorption in a homogeneous mixture of ^{238}U with an ideal moderator that gives an asymptotic spectrum. In this limit, any dips in the moderator caused by absorption in the resonance are small; we call this case "ideal." On the other hand, in a closely-packed lattice the flux in the moderator is very similar to that in the fuel, and the system is equivalent to a homogeneous mixture of ^{238}U with water. Resonance dips in the moderator flux become very evident.

The original NJOY flux calculator only solved the "ideal" case. A new version has now been written that will handle homogeneous mixes with real moderators. Some results are given in Table VIII. The homogeneous mix includes hydrogen only, and "NAI" refers to the original EPRI-CELL library produced by Nuclear Associates International. It is clear from the table that (1) the old NJOY results are somewhat off, possibly due to lack of convergence in the iterative solution used there; (2) that the differences between "ideal" and "hydrogen" are small, verifying the often-used assumption that resonances in ^{238}U are narrow with respect to scattering from hydrogen; and (3) that large differences between the LASL and NAI results remain.

As a further test of the flux calculator, we compared the LASL results with results obtained at Argonne National Laboratory (ANL) using the RABANL code.[35] The initial ANL results were very similar to the "NAI" column in Table VIII. Subsequent collaboration showed that these calculations did not include the potential scattering component for ^{238}U. This component is added later in the normal ANL fast reactor codes, but EPRI-CELL expects the potential component to be included. When the RABANL code was changed to include this contribution, the ANL results were very close to the LASL cross sections using the new NJOY flux calculator.

We conclude that the NJOY cross sections for the equivalent homogeneous cases are computed correctly. Disagreements between benchmark parameters computed using the NJOY cross sections and other sets must originate in other method

TABLE VIII

^{238}U ABSORPTION SHIELDING FACTORS AT 50 b BACKGROUND BY FOUR METHODS

Group[a]	Ideal	Hydrogen	Old NJOY	NAI
59	0.999	0.999	0.998	0.974
58	0.735	0.743	0.737	0.649
57	0.0495	0.0479	0.0498	0.0312
56	0.989	0.989	0.989	0.974
53	0.0593	0.0600	0.0578	0.0445
52	0.992	0.991	0.989	0.975
51	0.0510	0.0518	0.0451	0.0442
50	0.688	0.684	0.657	0.724
49	0.999	0.999	0.099	0.994
48	0.834	0.0830	0.0789	0.0757

[a]Quarter-lethargy GAM-I group structure. Group 57 contains the 6.7 eV resonance.

differences. Several candidates for the sources of these differences are presently being investigated.

E. Benchmark Spectra (R. B. Kidman)

The Cross Section Evaluation Working Group (CSEWG) fast reactor benchmarks[36] are extensively used by various laboratories for methods and data testing. Recently,[37] these 17 benchmarks were used to extensively test the following nuclear calculational systems at the Los Alamos Scientific Laboratory: ENDF/B-IV,[38] MINX,[39] 1DX,[40], 2DB,[41] ONETRAN,[42] and PERT-V.[43]

All of the cross sections, fluxes, and adjoints from those calculations were saved. During this last quarter the necessary codes were written to extract and numerically and graphically present desired spectra. The results have been compiled into a handbook called "SPECTRA-IV, Benchmark Spectra Based on LIB-IV." Graphical figures compare smooth interpolated curves for the central flux, edge flux, central adjoint, transport-reaction rate, and original cross-section averaging weighting function. Numerical tables compare spectra as computed with one- and two-dimensional diffusion theory and with one-dimensional $S_{16}P_{1/2}$ transport theory.

The handbook represents a further investigation of our data and methods and provides a convenient opportunity to collectively consider and study the spectra of all the benchmarks.

F. Neutron and Gamma-Ray Data for Activation Calculations (M. E. Battat and R. J. LaBauve)

A data library entitled GAMMON has been prepared that contains multigroup neutron cross sections and gamma-spectra data for use in activation calculations. The neutron data in GAMMON are the same as those in the MONTAGE-400 data package,[44] which lists 100-group cross sections for 421 reactions. These reactions can be characterized as follows:

- 197 reactions lead to radioactive products that are gamma-ray emitters. Because more than one reaction can lead to the same radionuclide, there are 107 unique reaction products.
- 161 reactions lead to important isomeric states, and no data are given for the half-lives and gamma-ray intensities of the reaction products. This is due to the fact that these reaction cross sections, almost all of which were calculated with the THRESH code,[45] include all final states. Of these 161 reactions, 75 are attributable to Sn (45) and Mo (30) isotopes. However, radioactive data are included for reactions that lead to the production of ^{92m}Nb, ^{177m}Lu, and ^{180m}Ta.
- 63 of the reactions result in radionuclides that are pure beta emitters.

Gamma-ray intensities (photons per 100 decays) were appended, where appropriate using a 25-group structure covering the range from 0 to 10 MeV. For each gamma-emitter, the gamma-ray energy (MeV) per disintegration was also supplied in the file. Gamma-ray intensities were derived from the rather complete tabulation (1313 radionuclides) complied by Erdtmann and Soyka[46,47] at Kernforschungsanlage (KFA) in Julich, Germany; a tape with these data was obtained from the Nuclear Data Section of the International Atomic Energy Agency (IAEA) in Vienna, Austria.

Work is in progress to extend the data in the GAMMON file to include maximum permissible concentrations (MPC) and absorbable decay energy. Testing of the library, by using it as input to an activation code, is also planned prior to making it available for general distribution.

On a more general note, we wish to point out that there may be many reactions in the GAMMON file that are not of interest to users of such data. For example, should the 51 reactions for Sn isotopes be retained in the file? What is needed to decide such matters is input from the fusion community as to the reactions of importance in their activation calculations, and we hope such input will

be forthcoming. This should result in a data set of much wider applicability than otherwise. Finally, for important reactions that result in isomeric states, one may be able to calculate the cross sections using more sophisticated nuclear systematic codes than were available when the MONTAGE file was first prepared.

III. FISSION PRODUCTS AND ACTINIDES: YIELDS, YIELD THEORY, DECAY DATA, DEPLETION, AND BUILDUP

A. Fission Yield Theory (R. Pepping and C. W. Maynard, University of Wisconsin; D. G. Madland, T. R. England, and P. G. Young)

The problem of evaluating the density of states for the many nuclei and nuclear shapes that may occur as fission fragments when the Moretto[48] prescription is being used has been simplified. The various thermodynamic functions required may be calculated independently and dimensionlessly for neutrons and protons in terms of the strength of the nuclear harmonic oscillator. The resultant expressions are smooth functions of the dimensionless temperature T_d and are well fit by cubic splines. The density at a given temperature for a particular nucleus may then be computed by evaluating the spline fit at the corresponding dimensionless temperature. This assumption has been tested and found to give worst case errors of the order of 0.1% at the lowest temperature, with agreement improving with excitation. The calculation was performed for proton and neutron numbers Z and N in the range $20 \leqslant Z \leqslant 80$, and $36 \leqslant N \leqslant 120$ on a dimensionless temperature grid of interval 0.015, with $0.028 \leqslant T_d \leqslant 0.462$. Single-particle levels were taken from Seeger's calculation for 39 prolate shapes on the ε, ε_4 grid.[49] Spline coefficients were computed and saved for each combination of particle number and shape and each type of particle. These coefficients have been used in all subsequent calculations.

The saddle-point method of evaluation of the convolution integral, which gives the unnormalized yield, has been investigated. The integral is

$$\int_0^G \rho(k) \int_0^{G-k} \rho_i(E_i)\rho_2(G-k-E_i)\,dE_i\,dk \quad ,$$

where $\rho(k)$ is the density of translational kinetic energy states, k is the prescission kinetic energy, $\rho_i(E_i)$ is the density of states of the i^{th} fragment excited by E_i, and G is the total energy to be partitioned. At values of $G \geqslant 5$ MeV, the saddle-point approximation gives results that agree to better than 10%

with a 7-point Newton-Cotes quadrature rule accurate to 1 part in 10^4. Agreement drops to 25% at G = 1 MeV. In making this comparison, the assumption has been made for simplicity that

$$\rho(E) = e^{2\sqrt{aE}} \quad , \qquad \rho(k) = k^{3/2} \quad ,$$

where a = A/9.5, and A = mass number.

Quantitative agreement with experimentally observed fission-product yields is currently being sought. To achieve this, yield data[50] have been lumped according to charge to minimize the effect of prompt neutrons. The data are averaged between a charge and the complimentary charge to estimate the fragment-charge yield (the difference found between the yield of a charge and the complimentary charge may indicate beta-decay contamination of the data). Yields are then computed for each fragment and compliment mass and charge for seven values of the spacing parameter δ,[51] between 1 and 7 fm, and the yields are lumped according to charge and δ. The log of the computed yields for a given Z are smooth in δ and may be well represented by cubic splines. Assuming some δ_0 and Z_0, charge yields may be used to determine a δ for each Z by solving for δ in

$$\frac{y_c(Z,\delta)}{y_d(Z)} = \frac{y_c(Z_0,\delta_0)}{y_d(Z_0)} \quad ,$$

where y_c and y_d are the computed yields and data, respectively. Choosing too small a δ_0 results in charge distributions for fixed mass that are too narrow and forces the scission-point shape to the prolate edge of the shape grid. Too large a δ_0 gives a small Coulomb energy and an unreasonable large scission-point separation. The choice of δ_0 and Z_0 is otherwise arbitrary.

Yields have been computed for the YMAX (maximum phase-space) and GMAX (minimum potential energy) cases, which have been described previously.[52] The YMAX method has been modifed here by requiring the YMAX configuration to occur in the immediate vicinity of the GMAX configuration. (The shape space is simply too large to compute a yield for all possible shape combinations.)

A new treatment of prompt neutrons has also been included. Previously, the average nuclear temperature T was computed, and the emission of monoenergetic neutrons of kinetic energy 2T was assumed to occur if energetically possible. Assuming a simple evaporation spectrum for the neutrons, a more realistic treat-

ment is possible. If a nucleus excited by energy E to a temperature T has a neutron separation energy S_1 and the resulting A-1 nucleus has a neutron separation energy of S_2, the probability of terminating the neutron-emission sequence, neglecting gamma competition, with one further neutron is given by

$$P_{stop} = C\int_{E-S_1-S_2}^{E-S_1} \frac{E_n}{T^2} \exp(-E_n/T)dE_n \quad ,$$

where C is a normalizing constant. The probability of continuing the sequence is $1-P_{stop}$. Average kinetic energies may be computed and the decay sequence continued.

Figures 8 and 9 illustrate this method for $^{235}U(n_{th},f)$. Assuming $Z_0 = 46$ and $\delta_0 = 2$ fm, $\delta(Z)$ was extracted. Assuming these $\delta(Z)$, yields were recomputed. Shown are the $\delta(Z)$, the fragment and charge yields, and the different product yields resulting from the two treatments of the prompt neutrons. Experimental data is taken from Ref. 50 and is plotted along with the computed yields for comparison.

In general, the YMAX yields are smoother than GMAX. With $\delta = 2$ fm, six to seven charges are yielded for a given fragment mass. The average Coulomb energy is about 158 MeV in both cases and about 10 MeV lower than desired. Regarding the adequacy of the shapes space, all but four fragment yields occurred at scission configurations with values of ε less than the allowed maximum $\varepsilon = 0.6$. However, almost all configurations occurred at the maximum prolateness allowed in the ε_4 degree of freedom. To extend the space in this degree of freedom would be to allow unphysical diamond-like shapes with relatively sharp corners. This result indicates that the two-parameter description is simply inadequate to describe fission-fragment shapes.

The computed prompt neutron number and total gamma energies resulting from this treatment are noteworthy.

	GMAX	YMAX
ν_p	3.95	4.20
E_γ (MeV)	5.42	5.01

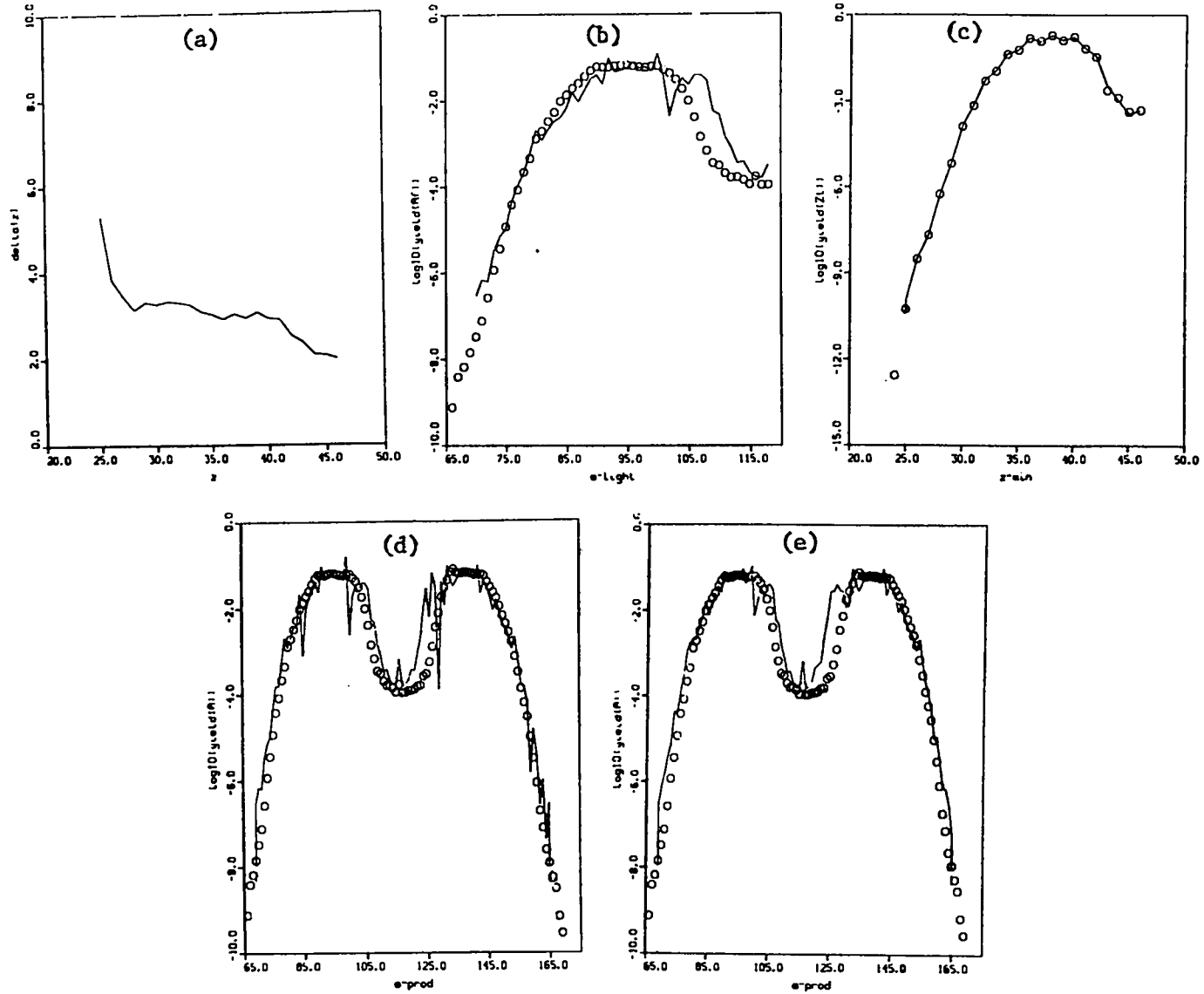

Fig. 8.

GMAX yields. Circles represent experimental fission product yields from Ref. 4. (a) $\delta(Z)$, (b) light fragment (pre-neutron emission) yields, (c) charge yields, (d) fission product yields assuming 2T neutron emission, and (e) fission product yields assuming elementary cascade model.

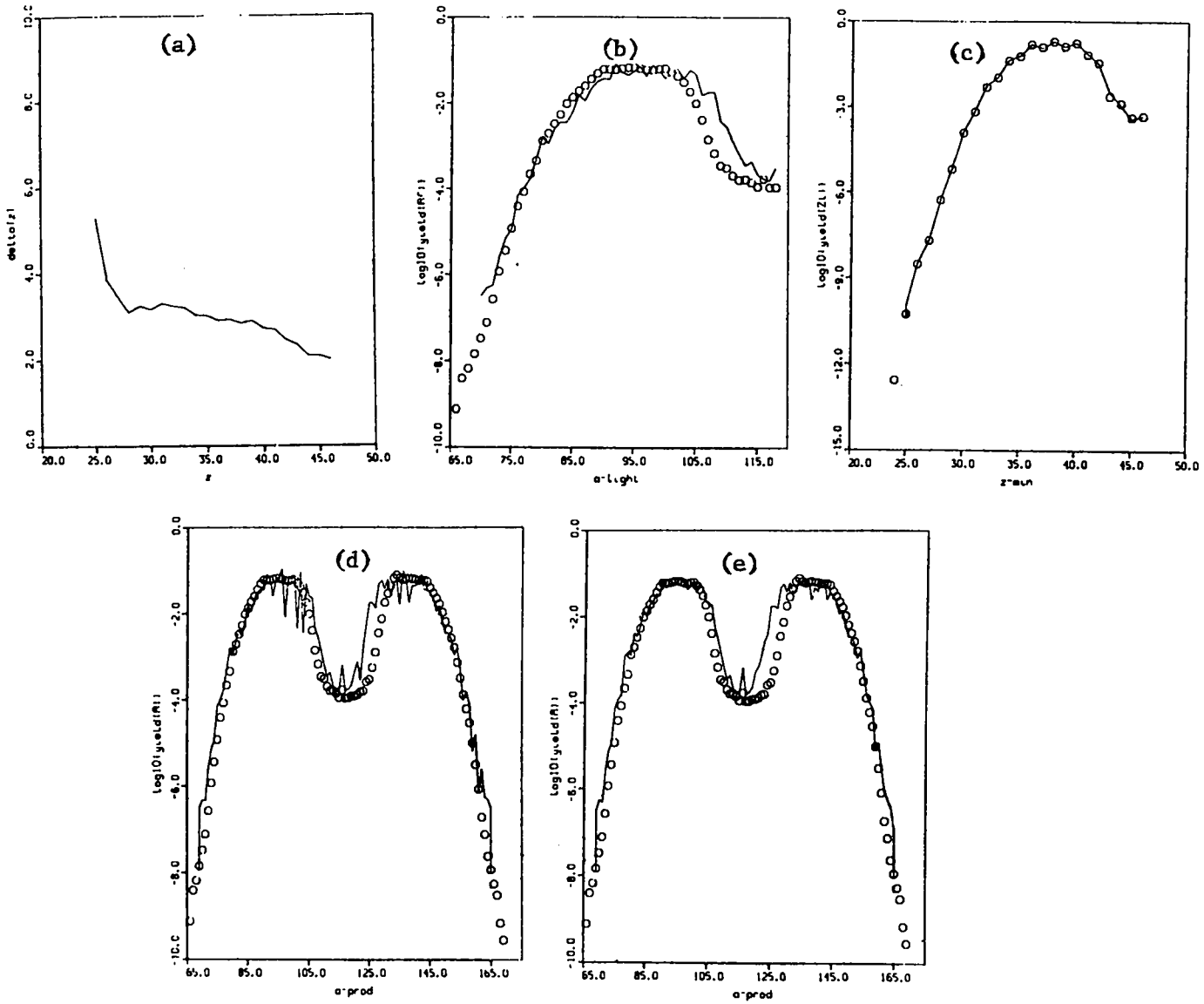

Fig. 9.
YMAX yields. Circles represent experimental fission product yields from Ref. 4. (a) $\delta(Z)$, (b) light fragment (pre-neutron emission) yields, (c) charge yields, (d) fission product yields assuming 2T neutron emission, and (e) fission product yields assuming elementary cascade model.

The prompt neutron yields are high by about 1.5 while the gamma energies are only about 1 MeV low. This would result from an excess 10-12 MeV of excitation energy, about the same amount as the deficit in the Coulomb energy. It is tempting to simply move this extra 10 MeV into translational kinetic energy such that, when added to the Coulomb energy, the total fragment kinetic energy would agree with experiment. However, such a shift requires justification. Arbitrary shifting would be equivalent to the introduction of a new parameter and is not being considered at this time.

B. ENDF/B-V Integral Yield Testing (T. R. England and N. L. Whittemore)

The new ENDF/B-V cumulative and independent yields were processed using ENDF/B-IV decay/absorption chains. The result was compared with the LASL calorimetric decay-heat experiment and earlier calcuations using all ENDF/B-IV data. Results were 1-3% smaller than in the earlier calculations (^{235}U thermal fission). We found that the nuclide density was ∿4% too small and traced the reason to new isomeric states in new yield data. This is being corrected, and a comparison will then be made for ^{235}U and ^{239}Pu heating.

The yield evaluation was reported at the American Chemical Society meeting in Hawaii in April 1979.

C. ENDF/B-V Decay Data (T. R. England, N. L. Whittemore, and W. B. Wilson

A Phase I review of the expanded spectral data, Version 2, was made. The code generating average beta, gamma, alpha, x-ray, etc., energies and Q values was expanded to include comparisons with ENDF/B-IV. A large number of errors or missing data were identified and the results transmitted to the Chairman of the CSEWG Fission-Product and Actinide Subcommittee. File corrections are in progress.

ENDF/B-V will include 877 fission products. Of the unstable nuclides, 269 will have detailed spectra data, and an additional ∿31 will have average beta energies based on beta strength functions. Thus, in addition to the expansion in the types of decay data, the number of nuclides having spectral data has been increased from 181 to ∿300.

D. Actinide Decay Power Calculations with EPRI-CINDER (W. B. Wilson; T. R. England; O. Ozer, Electric Power Research Institute; and D. E. Wessol, Idaho National Engineering Laboratory)

The magnitude of radioactive decay power following reactor shutdown is the sum of contributions from fission products, actinides, and structural-material activation products. The contribution to total decay power from actinides, produced by the transmutation of heavy metals in non-fission reactions, has been studied for three light-water reactors -- a PWR and a BWR fueled with typical low-enrichment ^{235}U, and a PWR fueled with ^{232}Th and low-enrichment ^{233}U (C. E. System 80). Calculations of actinide decay power were performed with the EPRI-CINDER code[53] and fission-product library,[54] using an actinide data library currently being developed for EPRI. Temporal composition-dependent cross sections were calculated with the EPRI-CELL code[55] for each irradiation history.

The actinide decay power for each reactor system following a 34 000 Mwd/MT was computed and compared to the fission-product decay power calculated with the DKPOWR code described in the following section. The actinide decay power during the first 10^6 seconds of shutdown of the ^{232}Th-^{233}U system is dominated by the decay of ^{233}Th and ^{233}Pa and was found to vary from 6.3 to 55% of the fission-product decay power. The actinide decay power during the first 10^5 seconds of shutdown of the ^{235}U-^{238}U fueled PWR/BWR systems is dominated by the decay of ^{239}U and ^{239}Np and was found to vary from 6 to 28% of the fission-product decay power.

The details of the calculations will be presented at the June 1979 meeting of the American Nuclear Society in Atlanta, GA.

E. Development of the DKPOWR Code for Calculating Fission-Product Decay Power (W. B. Wilson, T. R. England, and R. J. LaBauve)

The DKPOWR code has been developed for calculating fission-product radioactive decay power produced in reactor fuel following a user-specified irradiation history. Aggregate fission-product decay power is calculated by folding the input histogram fission history of each fissionable nuclide with an associated decay power pulse function f(t), describing the decay power at t seconds following a fission pulse. The pulse function description of fission-product decay power is a product of recent work pertinent to the development of the new 1978-79 American Nuclear Society (ANS) fission-product decay power standard[56] by the ANS 5.1 working group.

The DKPOWR code may be used to calculate the fission-product decay power and its uncertainty exactly as specified in the new standard. Options are available in the code to permit the use of alternative algorithms and assumptions in the calculation in anticipation of both questions on the consequences of assumptions used in the standard and, perhaps, the further development of the standard to include, e.g., additional pulse functions or alternative algorithms.

Documentation for the code is currently being developed for distribution by the Electric Power Research Institute.

REFERENCES

1. H. Rauch, "The Low Energy Neutron Scattering Lengths of He^3 and T and Their Relation to the Four-Body Problem," in Few Body Systems and Nuclear Forces I Proceedings, Graz 1978, H. Zingl, M. Haftel, and H. Zankel, Eds, (Springer-Verlag, New York, 1978), p. 289.

2. R. E. Donaldson, W. Bartolini, and H. Otsuki, "Measurement of the Coherent-Scattering Amplitude of Tritium," Phys. Rev. C5, 1952 (1972). NOTE: The value of a_c(n-T) usually quoted from this article is obtained using the "accepted" value of a_c(n-D). The value obtained using the authors' own determination of a_c(n-D) is a_c(n-T) = 3.53 $\pm$ 0.23 fm, in much better agreement with our results.

3. G. M. Hale and D. C. Dodder, "Charge-Independent R-Matrix Analysis of the Four-Nucleon System," in Few Body Systems and Nuclear Forces II Proceedings, Graz 1978, H. Zingl, M. Haftel, and H. Zankel, Eds., (Springer-Verlag, New York, 1978), p. 523.

4. V. P. Vertebnyi, M. F. Vlasov, A. L. Kirilynk, V. V. Kolotyi, H. V. Pasechnik, and V. A. Stephanenko, "Measurements of the Neutron Cross Sections of Tritium in the 0.007 to 5 eV Region," Izv. Akad. Naak SSSR, Ser. Fiz. 31, 349 (1967) [tranl.: Bull. Acad. Sci. USSR, Phys. Ser. 31, 334 (1967)].

5. F. O. Purser, Triangle Universities National Laboratory, personal communication; H. H. Hogue, P. L. VonBehren, D. H. Epperson, S. G. Glendinning, P. W. Likowski, C. E. Nelson, H. W. Newson, F. O. Purser, W. Tornow, C. R. Gould, and L. W. Seagondollar, "Differential Elastic and Inelastic Scattering of 6- to 15-MeV Neutrons from Beryllium," Nucl. Sci. Eng. 68, 38 (1978).

6. D. M. Drake, G. F. Auchampuagh, E. D. Arthur, C. E. Regan, and P. G. Young, "Double-Differential Beryllium Neutron Cross Sections at Incident Neutron Energies of 5.9, 10.1, and 14.2 MeV," Nucl. Sci. Eng. 63, 401 (1977).

7. D. I. Garber, L. G. Stromberg, M. D. Goldberg, D. E. Cullen, and V. M. May, "Angular Distributions in Neutron-Induced Reactions, Vol. I, Z = 1 to 20," Brookhaven National Laboratory report BNL 400 (1970).

8. R. O. Lane, A. S. Langsdorf, Jr., J. E. Monahan, and A. J. Elwyn, "Tables of Differential Cross Sections for Scattering of Neutron from Various Nuclei," Argonne National Laboratory report ANL-6172 (1960).

9. R. O. Lane, A. J. Elwyn, and A. Langsdorf, Jr., "Polarization and Differential Cross Section of Neutrons Scattered from Be^{9}: Parities of the 7.37- and 7.54-MeV States in Be^{10}," Phys. Rev. 133, 409 (1964).

10. A. Langsdorf, Jr., R. O. Lane, and J. E. Monahan, "Neutron Scattering Angular Distribution," Argonne National LAboratory report ANL-5567 (1956).

11. D. Wilmore and P. E. Hodgson, "The Calculation of Neutron Cross Sections from Optical Potentials," Nucl. Phys. 55, 673 (1964).

12. P. G. Young, L. Stewart, R. E. MacFarlane, and D. W. Muir, "n + ^{9}Be Cross Section Evaluation," in "Applied Nuclear Data Research and Development January 1-March 31, 1977," Los Alamos Scientific Laboratory report LA-6893-PR, p. 9 (1977).

13. E. D. Arthur and O. Bersillon, "Calculations of $^{191}Ir(n,\gamma)$ and $^{193}Ir(n,\gamma)$ Cross Sections," in "Applied Nuclear Data Research and Development October 1 - December 31, 1977," Los Alamos Scientific Laboratory report LA-7200-PR (1978), p. 7.

14. P. G. Young and E. D. Arthur, "GNASH: A Preequilibrium Statistical Nuclear Model Code for Calculation of Cross Sections and Emission Spectra," Los Alamos Scientific Laboratory report LA-6947 (1977).

15. C. L. Dunford, "A Unified Model for Analysis of Compound Nucleus Reactions," Atomic International Report AI-AEC-12931 (1970).

16. O. Bersillon, Bruyères-le-Châtel, personal communication (1978).

17. B. P. Bayhurst, J. S. Gilmore, R. J. Prestwood, J. B. Wilhelmy, Nelson Jarmie, B. H. Erkkila, and R. A. Hardekopf, "Cross Sections for (n,xn) Reactions between 7.5 and 28 MeV," Phys. Rev. C12, 451 (1975).

18. D. Drake, Los Alamos Scientific Laboratory, personal communication (1978).

19. C. Philis and E. D. Arthur, "Evaluation of the Tungsten Isotopes," in "Applied Nuclear Data Research and Development April 1 - June 30, 1978," Los Alamos Scientific Laboratory report LA-7482 (1978), p. 7.

20. A. B. Smith, Argonne National Laboratory, personal communication.

21. P. A. Guenther and A. B. Smith, "Fast Neutron Elastic and Inelastic Scattering from the Even Tungsten Isotopes," Bull. Am. Phys. Soc. 23, 944 (1978).

22. D. G. Foster, Jr., and Dale W. Glasgow, "Neutron Total Cross Sections 2.5 - 15 MeV, I. Experimental," Phys. Rev. C3, 576 (1971).

23. J. Delaroche, G. Haouat, R. Shamu, J. Lachkar, M. Patin, J. Sigaud, and J. Chardine, "Study of Even-Even Tungsten Isotopes by Neutron Scattering," Proc. of the National Conf. on Neutron Physics, Kiev (1977).

24. J. Jary and J. Frehaut, "Systematique des Sections Efficaces de Reaction (n,2n) pour des Series d'Isotopes Separes," Proc. Int'l. Conf. on Neutron Physics and Nuclear Data for Reactors and Other Applied Purposes, Harwell (1978), p. 1038.

25. David G. Madland and J. Rayford Nix, "Calculation of Prompt Fission Neutron Spectra," to be presented at the 1979 Annual Meeting of the American Nuclear Society, Atlanta, GA, in June, 1979.

26. D. G. Madland and J. R. Nix, "Calculation of Prompt Fission Neutron Spectra," in "Applied Nuclear Data Research and Development October 1 - December 31, 1978," Los Alamos Scientific Laboratory report LA-7722-PR (1979), p.11.

27. Ch. Lagrange, "Parameterization of the Optical Model from 10 keV to 20 MeV and an Application to the Spherical Nuclei ^{89}Y and ^{93}Nb," Proc. of the Third All-Union Conf. on Neutron Physics, Kiev, USSR, June 1975, Vol. III, p. 65, INDC(CCP)-99/G.

28. R. J. Barrett and R. E. MacFarlane, "Coupled Neutron and Photon Cross Sections for Transport Calculations," Los Alamos Scientific Laboratory report LA-7808-MS (1979).

29. R. E. MacFarlane and R. Prael, "Discrete Angle Representation of Thermal Neutron Scattering," in "Applied Nuclear Data Research and Development October 1 - December 31, 1978," Los Alamos Scientific Laboratory report LA-7722-PR (1979), p. 16.

30. M. T. Robinson, in Nuclear Fusion Reactors (British Nuclear Energy Society, London, 1970).

31. J. Lindhard, V. Nielsen, M. Scharff, and P. V. Thomsen, Kgl. Dansk. Vidensk. Selsk. Mat-Fys. Medd. 33 (1963).

32. D. M. Parkin and A. N. Goland, "Calculation of Radiation Effects As A Function of Incident Neutron Spectrum," in Radiation Effects (Gordon and Breach, Ltd., 1976).

33. T. A. Gabriel, J. D. Amburgey, and N. M. Greene, "Radiation-Damage Calculations: Primary Recoil Spectra, Displacement Rates, and Gas-Production Rates," Oak Ridge National Laboratory report ORNL/TM-5160 (1976).

34. Odelli Ozer, Electric Power Research Institute, personal communication.

35. H. Henryson, II, Argonne National Laboratory, personal communication.

36. H. Alter, R. B. Kidman, R. LaBauve, R. Protsik, and B. A. Zolator, "ENDF-202 Cross Section Evaluation Working Group Benchmark Specifications," Brookhaven National Laboratory report BNL-19302 (1974).

37. R. B. Kidman, "ENDF/B-IV, LIB-IV, and the CSEWG Benchmarks," Los Alamos Scientific Laboratory report LA-7355-MS (1978).

38. D. Garber, Ed., "Data Formats and Procedures for the ENDF Neutron Cross Section Library," Brookhaven National Laboratory report BNL 50274 (1976).

39. C. R. Weisbin, P. D. Soran, R. E. MacFarlane, D. R. Harris, R. J. LaBauve, J. S. Hendricks, J. E. White, and R. B. Kidman, "MINX, A Multigroup Interpretation of Nuclear X-Sections from ENDF/B," Los Alamos Scientific Laboratory report LA-6488-MS (1976).

40. R. W. Hardie and W. W. Little, Jr., "1DX, A One-Dimensional Diffusion Code for Generating Effective Nuclear Cross Sections," Battelle Northwest Laboratory report BNWL-954 (1969).

41. W. W. Little, Jr., and R. W. Hardie, "2DB User's Manual -- Revision 1," Battelle Northwest Laboratory report BNWL-831 REV 1 (1969).

42. T. R. Hill, "ONETRAN: A Discrete Ordinates Finite Element Code for the Solution of the One-Dimensional Multigroup Trasnport Equation," Los Alamos Scientific Laboratory report LA-5990-MS (1975).

43. R. W. Hardie and W. W. Little, Jr., "PERT-V, A Two-Dimensional Perturbation Code for Fast Reactor Analysis," Battelle Northwest Laboratory report BNWL-1162 (1969).

44. Radiation Shielding Information Center DLC-33/MONTAGE data package (1978).

45. S. Pearlstein, "Neutron-Induced Reactions in Medium Mass Nuclei," J. Nucl. Energy 27, 81 (1973).

46. G. Erdtmann and W. Soyka, "The Gamma-Ray Lines of Radionuclides, Ordered by Atomic and Mass Number. Part I. Z = 2-57 (Helium-Lanthanum)," J. Radioanal. Chem. 26, 375-495 (1975).

47. G. Erdtmann and W. Soyka, "The Gamma-Ray Lines of Radionuclides, Ordered by Atomic and Mass Number. Part II. Z = 58-100 (Ce-Fm)," J. Radioanal. Chem. 27, 137-286 (1975).

48. L. G. Moretto, "Statistical Description of Deformation in Excited Nuclei and the Disappearance of Shell Effects with Excitation Energy," Nucl. Phys. A182, 641 (1972).

49. P. A. Seeger and W. M. Howard, "Semiempirical Atomic Mass Formula," Nucl. Phys. A23, 491 (1975).

50. M. E. Meek and B. F. Rider, "Compilation ofFission Product Yields," Vallecito Nuclear Center report NEDO-12154 (1974).

51. R. E. Pepping, C. W. Maynard, D. G. Madland, T. R. England, and P. G. Young, "Fission Yield Theory," in "Applied Nuclear Data Research and Development, July 1 - September 30, 1978," Los Alamos Scientific Laboratory report LA-7596-PR (1978), p. 26.

52. R. E. Pepping, C. W. Maynard, D. G. Madland, T. R. England, and P. G. Young, "Fission Yield Theory," in "Applied Nuclear Data Research and Development, October 1 - December 31, 1977," Los Alamos Scientific Laboratory report LA-7200-PR (1978), p. 29.

53. T. R. England, W. B. Wilson, and M. G. Stamatelatos, "Fission Product Data For Thermal Reactors, Part 2: Users Manual for EPRI-CINDER Code and Data," Electric Power Research Institute report EPRI NP-356, Part 2 (Dec. 1976). Also published as Los Alamos Scientific Laboratory report LA-6746-MS (Dec. 1976).

54. T. R. England, W. B. Wilson, and M. G. Stamatelatos, "Fission Product Data for Thermal Reactors, Part 1: A Data Set for EPRI-CINDER Using ENDF/B-IV," Electric Power Research Insititute report EPRI NP/356, Part 1 (Dec. 1976). Also published as Los Alamos Scientific Laboratory report LA-6745-MS (Dec. 1976).

55. "ARMP: Advanced Recycle Methodology Program," Electric Power Research Institute report CCM-3 (Sept. 1977) (Proprietary), Chapter 5, Part II, "EPRI-CELL Code Description."

56. American Nuclear Society Proposed ANS 5.1 Standard, "Decay Heat Power in Light Water Reactors," (June 1978) (Rev. through March 19, 1979).